


ORIGINAL ARTICLE

Neural Dynamics of Reward-Induced Response Activation and Inhibition

Lihui Wang^{1,2,3}, Wenshuo Chang ¹, Ruth M. Krebs⁴, C. Nico Boehler⁴, Jan Theeuwes^{2,5} and Xiaolin Zhou^{1,6,7,8,9}

¹School of Psychology and Cognitive Sciences, Peking University, Beijing 100871, China, ²Department of Experimental and Applied Psychology, Vrije Universiteit, 1081 BT Amsterdam, The Netherlands, ³Department of Experimental Psychology, Institute of Psychology II, Otto-von-Guericke University, Universitätsplatz 2, 39016 Magdeburg, Germany, ⁴Department of Experimental Psychology, Ghent University, Henri Dunantlaan 2, 9000 Ghent, Belgium, ⁵Institute Brain and Behavior Amsterdam (iBBA), Amsterdam, The Netherlands, ⁶Key Laboratory of Machine Perception (Ministry of Education), Peking University, Beijing 100871, China, ⁷Beijing Laboratory of Behaviour and Mental Health, Peking University, Beijing 100871, China, ⁸Institute of Psychological and Brain Sciences, Zhejiang Normal University, Zhejiang 321004, China and ⁹PKU-IDG/McGovern Institute for Brain Research, Peking University, Beijing 100871, China

Address correspondence to Xiaolin Zhou, School of Psychological and Cognitive Sciences, Peking University, Beijing 100871, China. Email: xz104@pku.edu.cn

Abstract

Reward-predictive stimuli can increase an automatic response tendency, which needs to be counteracted by effortful response inhibition when this tendency is inappropriate for the current task. Here we investigated how the human brain implements this dynamic process by adopting a reward-modulated Simon task while acquiring EEG and fMRI data in separate sessions. In the Simon task, a lateral target stimulus triggers an automatic response tendency of the spatially corresponding hand, which needs to be overcome if the activated hand is opposite to what the task requires, thereby delaying the response. We associated high or low reward with different targets, the location of which could be congruent or incongruent with the correct response hand. High-reward targets elicited larger Simon effects than low-reward targets, suggesting an increase in the automatic response tendency induced by the stimulus location. This tendency was accompanied by modulations of the lateralized readiness potential over the motor cortex, and was inhibited soon after if the high-reward targets were incongruent with the correct response hand. Moreover, this process was accompanied by enhanced theta oscillations in medial frontal cortex and enhanced activity in a frontobasal ganglia network. With dynamical causal modeling, we further demonstrated that the connection from presupplementary motor area (pre-SMA) to right inferior frontal cortex (rIFC) played a crucial role in modulating the reward-modulated response inhibition. Our results support a dynamic neural model of reward-induced response activation and inhibition, and shed light on the neural communication between reward and cognitive control in generating adaptive behaviors.

Key words: LRP, MFC, response control, reward, theta-band oscillation

Introduction

It is crucial for humans to coordinate between automatic (i.e., bottom-up) and goal-directed (i.e., top-down) behavioral

tendencies. A growing body of studies has shown that both the bottom-up and the top-down cognitive processing can be modulated by reward (Awh et al. 2012; Yee and Braver 2018), the

driving force of human behavior (Berridge and Robinson 1998). On the one hand, stimuli that are associated with reward attract visual attention (Theeuwes and Belopolsky 2012; Wang et al. 2013) and provoke motor reactions (Bundt et al. 2016). On the other hand, reward expectation improves task performance by motivating the inhibition of task-irrelevant information (Padmala and Pessoa 2011; Kang et al. 2017). Although the bias for reward can be beneficial in an evolutionary sense, it nevertheless causes undesirable behavioral consequences when it is in conflict with the current goals (Dayan et al. 2006). Thus, top-down cognitive control needs to overcome such prepotencies to realize task goals and ensure healthy functioning (Hare et al. 2011; Boehler et al. 2012). Despite the increasing number of studies that focus either on the reward-modulated cognitive bias or on the reward-modulated inhibitory control, it remains unclear how the conflict between these 2 processes is resolved in the brain, and how reward-seeking and cognitive control are coordinated to generate adaptive behaviors (Kouneiher et al. 2009; Botvinick and Braver 2015; Westbrook and Braver 2016).

In recent studies, a 2-stage model was proposed to describe the coordination between response tendencies towards reward and the top-down control on such response tendencies (Freeman et al. 2014; Freeman and Aron 2016). According to this model, reward-predicting stimuli induce an early motor activation, which is then inhibited by a control process when this response is inappropriate for the current goal. Specifically, in a Go/NoGo task, relative to reward-unrelated NoGo stimuli, more commission errors occurred to reward-related NoGo stimuli and the effector-muscle activity to reward-related NoGo stimuli was enhanced in an early time window but was soon inhibited in a late time window (Freeman et al. 2014; high-reward vs. low-reward in Freeman and Aron 2016). Although the 2-stage model and the underlying empirical work have provided valuable insights into the dynamic control of reward-induced response tendencies, it was established mainly based on evidence from the Go/NoGo task which reflects the neurocognitive process that countermands a response tendency (Aron et al. 2016). The generality of this model therefore needs to be verified with evidence from more complex tasks, which engage the detection of competing responses and the selective inhibition of inappropriate responses (i.e., in situations in which the response control is not only required by the task at hand but also motivated to obtain reward; Forstmann et al. 2008; Salzer et al. 2017). Moreover, the neural mechanism of this dynamic process needs to be elucidated more clearly.

Here we addressed these issues by using the Simon task (Simon 1969; Hommel 2011; Salzer et al. 2017) and by investigating the neural dynamics of reward-induced response activation and inhibition. In particular, we aimed to reveal the brain networks involved in the 2 processing stages, and the temporal coherence (Fries 2005) and connectivity (Friston 2009) between the networks.

The Simon effect refers to a spatial congruency effect in which a response to a lateral target is slowed down when the target location does not correspond spatially with the motor response (e.g., left vs. right hand) (Simon 1969; Hommel 2011). An influential model proposes that the target location automatically generates a spatially corresponding response code via a stimulus-driven route (Eimer 1995), while the correct response code is produced along a controlled pathway following the instructed stimulus–response mapping. When the 2 response codes converge, behavioral performance is enhanced; otherwise performance is impaired (De Jong et al. 1994; Zhang and Kornblum 1997). The automatic response activation, including

the activation of its motor component, takes effect soon after target onset, dissipates quickly over time (De Jong et al. 1994) and can be overcome by an active suppression when the response activation conflicts with the response code required by the task set (Ridderinkhof 2002; Forstmann et al. 2008; Proctor et al. 2011). As a result, the Simon effect decreases as the response speed slows down, showing a decreasing function between the size of the Simon effect and the response speed. The slope of the decrease function is perceived as an indicator of the decay of the automatic response activation (De Jong et al. 1994; Wiegand and Wascher 2005). Hence, as an extension of the Go/NoGo task, the Simon task enables us to investigate the temporal profile of the response activation that is automatically triggered by the stimulus, and the corresponding response inhibition when this activated response is in conflict with the task goal.

In the current study, we associated high or low reward with a lateral target, the location of which was either congruent or incongruent with the correct response hand. We expected a larger Simon effect for a high-reward than for a low-reward target, as the target predicting a high reward is likely to induce stronger automatic response activation based on its (task-irrelevant) location, regardless of whether this response activation is congruent or incongruent with the correct response hand. When this enhanced response activation is in conflict with the correct response hand (in the incongruent condition), stronger response inhibition has to be recruited to overcome this enhanced response tendency for the performance actually gaining the reward. To this end, we conducted 2 behavioral experiments with different stimuli (letter in Experiment 1A and digit in Experiment 1B) to show how the Simon effect would be affected by reward. By analysing the decrease function of the Simon effect, we investigated the underlying mechanisms of how reward modulates the temporal profile of the response activation. Building on our behavioral studies, we used EEG (Experiment 2) and fMRI (Experiment 3) to reveal the temporal and spatial dynamics of reward-induced response activation and inhibition in the brain. For the reward-induced response activation, we predicted that high-reward targets would induce greater BOLD signals in the motor cortex as well as stronger lateralized readiness potentials (LRP), an ERP component reflecting response preparation (van Turennout et al. 1998; Töllner et al. 2012), driven by the early activation of the motor cortex by target location. For the top-down control of inhibiting the inappropriate response activation, high-reward targets would induce stronger theta-band oscillation in medial frontal cortex (MFC), a well-documented component for conflict monitoring and cognitive control (Cavanagh and Frank 2014; Cohen 2014), and enhanced neural activity in presupplementary motor area (pre-SMA) and right inferior frontal cortex (rIFC), 2 key brain regions in the neural pathway for response inhibition (Aron and Poldrack 2006; Aron et al. 2007; Forstmann et al. 2008; Boehler et al. 2010).

Prominent models suggest that response control is initiated via the connectivity between the frontal network (e.g., pre-SMA and rIFC) and the basal ganglia (Hikosaka and Isoda 2010; Neubert et al. 2010; Jahfari et al. 2011; Aron et al. 2016). However, there is no agreement on how reward and cognitive control integrate in the human brain to regulate response control. One account is that the prefrontal cortex, especially pre-SMA/dorsal anterior cingulate cortex (dACC), combines reward information and the current demand for control (Kouneiher et al. 2009; Shenhav et al. 2013), and engages the lateral prefrontal cortex to regulate action selection (Kouneiher et al. 2009). Another model is that reward modulates response

inhibition by tuning the frontosubthalamic pathway. For example, Herz et al. (2014) found that stimulating pre-SMA improves response inhibition when a reward delivery is expected, and this reward-modulated response inhibition is mediated by the enhanced connectivity between rIFC and subthalamic nucleus (STN). In the current study, we tested these models with dynamic causal modeling (DCM, Friston et al. 2003) in the fMRI experiment. We hypothesized that, if reward acts on the frontal pathway to modulate response control (Kouneiher et al. 2009; Duvernoie and Koehlin 2017), reward modulations would be observed only on the connectivity between pre-SMA and rIFC. If reward acts on the frontobasal ganglia pathway (Herz et al. 2014), reward modulations would be observed only on the connectivity from frontal areas to basal ganglia areas. In addition, there is a third possibility that reward interacts with cognitive control in both the frontal and frontobasal ganglia pathways. From this perspective, we would observe reward modulations on both the frontal pathway (pre-SMA and rIFC) and the fronto-basal ganglia pathway.

Materials and Methods

Participants

A total of 20 right-handed students at the Vrije Universiteit Amsterdam participated in Experiment 1A (8 females, 12 males, mean age 22.3 years). Overall, 20 right-handed students at Peking University participated in Experiment 1B (11 females, 9 males, mean age 20.2 years). Another 25 right-handed students at Peking University, who did not participate in Experiment 1B, took part in the EEG experiment (Experiment 2). One participant of the EEG experiment was excluded due to excessive artifacts (60% of the total trials), leaving 24 participants (8 females, mean age 21.9 years) for data analysis. A new group of 26 right-handed students at Peking University, who did not participate in Experiments 1B and 2, participated in the fMRI experiment (Experiment 3). Two of them were excluded due to excessive head movement (>3 mm), leaving 24 participants (14 females, mean age 21.1 years). All participants had normal or corrected-to-normal visual acuity and color vision. Written informed consents were obtained from each participant. This study was performed in accordance with the

Declaration of Helsinki and was approved by the Ethics Committee of the Department of Cognitive Psychology, Vrije Universiteit Amsterdam, and the School of Psychological and Cognitive Sciences, Peking University.

Stimuli and Design

In Experiments 1A, 2, and 3, stimuli were black letters “E” and “P” ($1.2^\circ \times 1.5^\circ$ in visual angle) presented against a gray screen. Each letter was surrounded by a red or blue circle (1.8° diameter). A black cross ($0.5^\circ \times 0.5^\circ$ in visual angle) was presented at the center of the screen for central fixation. For a specific trial, 1 of the 2 target letters was presented left or right to the central fixation (4° distance). Participants were required to discriminate the identity of the letter (“E” vs. “P”) by pressing the corresponding button on the keyboard with the left and right index finger, respectively. The position of the keyboard was fixed during the whole experiment, to ensure that the button “E” and the button “P” on the keyboard had equal horizontal distance to the midline of the screen. Thus, the response hand could be either congruent or incongruent with the spatial position of the letter. In Experiments 1A, 2, and 3, different reward magnitudes were associated with the identity (“E” vs. “P”) of the target letter (Fig. 1A). For half of the participants, letter “E” was associated with high reward, and letter “P” was associated with low reward; for the other half, the association was reversed. The color of the circle was irrelevant to both the task and the reward association.

To test the generality of the observed effects for different stimuli, we conducted Experiment 1B, where stimuli were black digits ‘3’, ‘4’, ‘5’, and ‘6’ ($1.2^\circ \times 1.5^\circ$ in visual angle) presented against a gray screen. A black cross ($0.5^\circ \times 0.5^\circ$ in visual angle) was presented at the center of the screen for central fixation. For a specific trial, one of the 4 digits was presented left or right to the central fixation (4° distance). Participants were required to discriminate the disparity of the digit (odd vs. even) by pressing the corresponding button (“E” vs. “P”) on the keyboard with the left and right index finger, respectively. Different reward magnitudes were associated with the disparity of the presented digit (Fig. 1B). For half of the participants, odd digit was associated with high reward while even digit was associated with low reward; for the other half, the association was reversed.

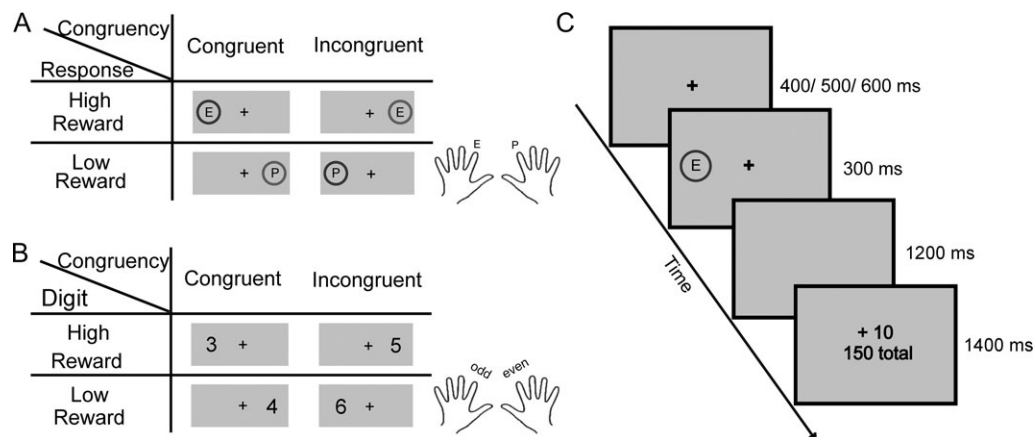


Figure 1. The design (A and B) and stimuli sequence (C) of the 4 experiments. In Experiments 1A, 2, and 3, high- or low-reward was associated with the identity of the target. The task was to discriminate the identity of the target letter (“E” vs. “P”), using the left and right index finger respectively (A). The location of the target could be either congruent or incongruent with the correct response hand. In Experiment 1B, the task was to discriminate the disparity of the digit (‘3’, ‘4’, ‘5’, or ‘6’). High- or low-reward was associated with the disparity of the target (odd vs. even) (B). A feedback frame was presented to indicate the points participants earned in the current trial and the total points the participant earned from the first trial (C).

Therefore, all the experiments had a 2 (reward: high vs. low) \times 2 (spatial congruency: congruent vs. incongruent) design, rendering to 4 experimental conditions: high-reward congruent (HC), high-reward incongruent (HIC), low-reward congruent (LC), and low-reward incongruent (LIC). Given that the mapping between the response button and response hand was fixed (left index finger for “E” and right index finger for “P”), while the mapping between reward association and response hand was counterbalanced across participants such that high-reward was associated with the left hand and low-reward was associated with the right hand for half of the participants whereas the association was reversed for the other half of the participants, any interaction between reward and spatial congruency cannot be reduced to handness.

The association between letter/digit and monetary reward was established by presenting a feedback frame after button press indicating the points a participant could receive in that trial. The earned points in each trial were calculated as $(1000 - RT) \times 0.002 \times \text{bonus_multiplier}$. For high-reward targets, *bonus_multiplier* was always 10; for low-reward targets, *bonus_multiplier* was always 1 (Le Pelley et al. 2015). Errors, trials with responses slower than 1000 ms resulted in no points.

Procedures

In Experiments 1 (behavioral) and 2 (EEG), participants were tested individually in a soundproof and dimly lighted room. They were seated in front of a monitor screen with their head positioned on a chin rest and were required to fix at the central cross throughout each trial. The eye-to-monitor distance was fixed at 65 cm. In Experiment 3 (fMRI), stimuli were presented through an LCD projector onto a rear screen located behind the participant’s head, and the participant viewed the screen via an angled mirror mounted on the head-coil of the MRI setup.

Each trial began with the presentation of the central fixation for a variable duration. The variable duration was 400/500/600 ms in Experiments 1 and 3, and was randomly jittered from 400 to 800 ms (for baseline correction of EEG data) in Experiment 2 (Fig. 1C). The target was then presented for 300 ms, followed by a blank screen. The blank screen lasted for up to 1200 ms until response was given. After response or the time limit (1200 ms) of the blank screen was reached, a feedback frame was presented and remained on the screen for 1400 ms. The feedback frame contained both the points in that trial and the total points accumulated from the beginning. In Experiment 1, the feedback frame was presented on every single trial. In Experiments 2 and 3, the feedback frame was presented after every 10 trials indicating both the points from the last 10 trials and the total points. The intertrial interval (ITI) was a blank screen of 1000 ms in Experiments 1, was jittered from 1250 to 2000 ms (1250/1500/1750/2000 ms) in Experiment 2, and was jittered from 2000 to 2750 ms (2000/2250/2500/2750 ms) in Experiment 3. The longer ITI in Experiment 3 was to accommodate to the temporal resolution of MRI scanning (TR = 2000 ms). There were 120 trials for each of the 4 experimental conditions. The 480 trials were divided into 10 blocks of equal length (48 trials), with each block including equal numbers of trials for each condition (12 trials). Trials from different conditions in each block were mixed and presented in a random order. At the end of each block, the total points and the corresponding amount of money calculated from the total points were presented on the screen. Participants were explicitly informed about the association between different targets and different levels of reward, and were encouraged to respond as

quickly and accurately as possible to maximize their bonus income. They were told that the points accumulated during the experiment would be proportionally exchanged into money and added to their basic payment (Experiment 1A: €6; Experiment 1B: 20 yuan, about €3; Experiments 2 and 3: 70 yuan, about €10). Overall, 20 practice trials were provided prior to the actual experiment.

Statistical Analysis of Behavioral Data

For each experimental condition, omissions, incorrect responses, and trials with RTs beyond the mean RT \pm 3 SD for all the correct trials were first excluded. Mean RT of the remaining trials (93.5% in Experiment 1A, 91.6% Experiment 1B, 91.6% in Experiment 2, and 94.9% Experiment 3) in each condition was then computed. The error rate in each condition was calculated as the proportion of the number of omissions and incorrect trials against the total number of trials in each condition.

Distributional analysis was then carried out on the Simon effect across different response speeds (De Jong et al. 1994). For each participant, valid trials in each experimental condition (correct trials with an RT within 3 SD of the mean RT in a particular condition) were divided into 6 RT bins, with equal numbers of trials in each bin. Mean RT was computed for each bin. In both the high-reward and low-reward conditions, the spatial congruency effect in each bin was obtained by subtracting the mean RT in the congruent condition from the mean RT in the incongruent condition. Linear regression between the spatial congruency effect and the mean RT in each bin was conducted. For each participant, a linear regression function $Y = a + b * (RT - RT_{avg})$ was fitted to the high-reward and the low-reward Simon effect-response speed function, respectively. The RT_{avg} was calculated by averaging RTs across all the conditions and participants (De Jong et al. 1994). The sixth bin was excluded from the regression analysis because of a larger variance for this bin than for any other bin (Wascher et al. 2001). To examine how the automatic activation of the spatial code and its decay were modulated by reward, the parameter estimates (the intercept *a* and the slope *b*) of the model fitting were compared between high-reward and low-reward conditions. Given that the larger Simon effects caused by reward manifested only in terms of RT but not in terms of error rates, probably due to a floor effect of error rates, the distribution analysis was conducted only for RTs.

EEG Recording

EEG was recorded from 64 Ag/AgCl-electrodes mounted in an elastic cap (Anticap Brain Products, Germany). The electro-oculogram (EOG) was recorded at 2 electrode sites: vertical EOG was monitored from an electrode placed above the right eye, and horizontal EOG from an electrode located at the outer canthus of the left eye. All electrode impedances were kept below 5 k Ω . The EEG and EOG recordings were amplified by BrainAmps (Brain Products, Germany) using a band-pass filter of 0.016–100 Hz, and digitized online at a sampling rate of 500 Hz. The EEG from all channels were online referenced to the nose electrode. The EEGLAB toolbox (Delorme & Makeig 2004) was used to denoise and segment EEG data. The data were high-pass filtered offline above 0.5 Hz, low-pass filtered below 30 Hz, and referenced to the average of all channels except the vertical and horizontal EOG. Ocular artifacts were corrected by a procedure based on independent component analysis (Jung et al. 2000; Drisdelle et al. 2017).

Event-Related Potential Analysis

For event-related potential (ERP) analysis, we focused on both the stimulus-locked LRP, which is time-locked to the onset of the stimulus, and the response-locked LRP, which is time-locked to the onset of the response (Töllner et al. 2012) to show the reward-induced response activation. In each trial, stimulus-locked epochs were extracted from the interval of -200 to 800 ms relative to stimulus onset, while response-locked epochs were derived from the interval of -1000 to 200 ms relative to response onset. Note here that none of the response-locked epochs had overlap with the epoch of the previous trial or the next trial, because all of the RTs (after the exclusion of outliers) were within the range of 211 – 768 ms. For stimulus-locked epochs, baseline corrections were applied to the interval of -200 to 0 ms relative to the stimulus onset. For response-locked epochs, baseline corrections were applied to the interval of -1000 to 800 ms relative to response onset, ensuring that the baseline had no overlap with the presentation of the target. Trials with mean voltages of epochs exceeding $\pm 70 \mu\text{V}$ were excluded to avoid artefact contamination (3% of the total trials for stimulus-locked epochs, and 9% of the total trials for response-locked epochs).

LRPs were obtained by subtracting ERP signals recorded at the ipsilateral motor cortex (C3/C4 electrode) of the correct response hand from ERP recorded at the contralateral motor cortex. For example, if the left hand was the correct response in a given trial, LRP was obtained by subtracting signals recorded at C3 from signals recorded at C4. If the right hand was the correct response, LRP was obtained by subtracting signals recorded at C4 from signals recorded at C3. For each condition, the obtained LRP was averaged across 2 both hemispheres (van Turennout et al. 1998).

The peak amplitude of stimulus- and response-locked LRP was identified at the group level in each of the 4 conditions. For stimulus-locked LRP, the peak detection started from 200 ms poststimulus onset. The mean amplitude was then calculated by averaging 50 points (100 ms) centered at the peak point (HC: 200 – 300 ms, HIC: 192 – 292 ms, LC: 194 – 294 ms, LIC: 190 – 290 ms). We labeled this time range as the early time window for stimulus-locked LRP, and extracted the amplitude from the following 100 -ms time range as the late time window (HC: 300 – 400 ms, HIC: 292 – 392 ms, LC: 294 – 394 ms, LIC: 290 – 390 ms). For response-locked LRP, the peak detection started from response onset and went backwards. The mean amplitude was calculated by averaging 50 points centered at the group peak point (HC: -118 to -18 ms, HIC: -108 to -8 ms, LC: -112 to -12 ms, LIC: -114 to -14 ms). This time range was labeled as the late time window for response-locked LRP, and the 100 -ms time range prior to this late time window was labeled as the early time window (HC: -218 to -118 ms, HIC: -208 to -108 ms, LC: -212 to -112 ms, LIC: -214 to -114 ms). For both stimulus- and response-locked LRP, we expected that the amplitude would be enhanced in high-reward conditions relative to low-reward conditions in the early time window, and this reward modulation would be attenuated in the late time window.

Time Frequency Analysis

For each trial in each condition, time–frequency transformation was performed by convolving the induced activity with a complex Morlet wavelet with a Gaussian kernel of 4-cycle width using Fieldtrip (Oostenveld et al. 2011). This procedure was applied to frequencies ranging from 2 to 30 Hz in steps of 1 Hz, during the time window of -700 to 1200 ms relative to stimulus

onset in steps of 10 ms. Event-related power changes were calculated as the percentage change of power relative to the baseline (-200 to 0 ms relative to stimulus onset).

Given the well-documented role of frontal theta oscillation in conflict resolution (Nigbur et al. 2012; Cavanagh and Frank 2014; Töllner et al. 2017), statistical analyses were focused on the theta-band activities in the frontal areas. The theta oscillatory activities were extracted within the frequency of 6 – 8 Hz during the time window of 0 – 800 ms poststimulus onset. Cluster-based permutation tests (Maris and Oostenveld 2007) were implemented on the frontocentral channels (Fz, F1, F2, F3, F4, F5, F6, FCz, FC1, FC2, FC3, FC4, FC5, FC6, Cz, C1, C2, C3, C4, C5, and C6). Dependent-sample t tests on incongruent trials versus congruent trials were conducted for each channel. To investigate whether and how the theta oscillation driven by the response conflict was modulated by reward, the t tests between incongruent and congruent trials were carried out for the high-reward condition and the low-reward condition, respectively. The interaction between reward and congruency were further tested by conducting a cluster-based permutation t test comparing the differences between the contrast “HIC > HC” and the contrast “LIC > LC”. Adjacent channels exceeding alpha level (0.05) were grouped into a cluster. Cluster-level statistic was calculated by taking the sum of the t -values within the cluster. The number of random permutations using Monte Carlo method was set to 5000 .

fMRI Data Acquisition and Preprocessing

For each participant, $T2^*$ -weighted echo-planar images (EPI) with blood oxygenation level-dependent (BOLD) contrast was obtained with a research-dedicated GE MR750 3T scanner (General Electric, Fairfield, CT). In total, 33 transversal slices of 4 mm thickness that covered the whole brain were acquired in an interleaved order (repetition time: 2000 ms, echo time: 30 ms, field of view: 192 mm \times 192 mm, in-plane resolution: 3 mm \times 3 mm, flip angle: 90°). The whole functional scanning session included 10 runs for the 10 blocks of the experiment, with each run containing 138 EPI volumes. A high-resolution, whole-brain structural scan (1 mm³ isotropic voxel MPRAGE) was acquired after functional imaging. Data of one run from one participant was excluded from analysis because of technical error during the scanning, and the behavioral data from this block (run) was also excluded.

Data were preprocessed with the Statistical Parametric Mapping software SPM8 (Wellcome Trust Department of Cognitive Neurology, London, UK). For each run, the first 5 volumes were discarded to allow for $T1$ equilibration effects. Preprocessing was done with SPM8 default settings. Images from each run were slice-time corrected and motion corrected. Different brain tissues (gray matter, white matter, and cerebrospinal signals) were segmented following standard procedures implemented in SPM8 and were transformed into standard MNI space and resampled to $3 \times 3 \times 3$ mm³ isotropic voxel. The data were then smoothed with a Gaussian kernel of 6 mm full-width half-maximum (FWHM) to accommodate intersubject anatomical variability.

Statistical Analysis of fMRI Data

Data were high-pass filtered with a cutoff period of 128 s and corrected for serial correlation. We specified a general linear model (GLM) to construct a multiple regression design matrix, with each of the 4 experimental conditions (HC, HIC, LC, LIC)

being modeled as separate regressors. The 4 event types were time-locked to the stimulus onset, and modeled by an impulse function convolved with a canonical synthetic hemodynamic response function and its time derivatives (Friston et al. 1998; Hopfinger et al. 2000). To control for any potential confounding effect caused by response latency (especially given that correlation analysis between RT and parameter estimates would be conducted), a parametric modulation regressor of the mean-corrected RT (mean RT in a specific trial minus mean RT averaged across all trials in an experimental condition) was included for each experimental condition (Wang et al. 2015). The excluded trials (incorrect trials and outliers) were modeled as a regressor of no interest. The 6 head movement parameters derived from the realignment procedure were also included as regressors of no interest. Parameter estimates were subsequently calculated for each voxel using weighted least squares to provide maximum likelihood estimators based on the temporal autocorrelation of the data.

For each participant, we defined the contrast of “HIC > LIC” to identify brain areas involved in coping with response conflict that was modulated by reward. However, the contrast of “HIC > LIC” would likely identify brain areas reflecting both reward-induced response activation and the corresponding response inhibition. To disentangle these 2 processes and reveal the brain areas that are specifically related to reward-modulated response inhibition, we identified the brain areas only involved in the reward-enhanced response activation by the contrast of “HC > LC”, because the congruent condition did not require the inhibitory control, and further excluded these areas from the contrast of “HIC > LIC” through exclusive masking. The obtained contrast images of the first level analysis were entered into a second level random effect group analysis. Simple *t* tests were used to assess the specific effects. Areas of activation were identified as significant only if they passed the threshold of $P < 0.001$, family wise (FWE)-corrected at the cluster level, each voxel in the cluster significant at $P < 0.001$ uncorrected. To achieve a conservative criterion for the overall masking procedure, the threshold for the contrast of “HC > LC” that was used to mask the contrast of “HIC > LIC” was set to a quite liberal $P < 0.01$ uncorrected at the voxel level without any correction at the cluster level.

To identify primary motor cortex (M1), we specified another GLM. Events of trials with left-hand response and right-hand responses were modeled as separate regressors. Left M1 was identified by the contrast “Right-hand response > Left-hand Response” and right M1 was identified by the contrast “Left-hand response > Right-hand response.” Parameter estimates for the 4 experimental conditions were extracted from the 3-mm-radius sphere centered on the peak voxel in left M1 ($x = -42$, $y = -31$, $z = 43$) and right M1 ($x = 39$, $y = -22$, $z = 61$). The parameter estimates from M1 that was contralateral to the correct response hand and the parameter estimates from M1 that was ipsilateral to the response hand (i.e., contralateral to the incongruent targets) were entered into a 2×2 repeated-measures ANOVA, respectively. In addition, correlation analysis across participants was conducted between the reward-induced response activation and inhibition in M1, to test whether the inhibition strength depended on the activation strength as predicted by the 2-stage model (Freeman and Aron 2016). Specifically, the response activation strength was calculated in terms of the difference in parameter estimates between HC and LC from the contralateral M1. The response inhibition strength was calculated in terms of the difference in parameter estimates between LIC and HIC from the ipsilateral M1.

Dynamic Causal Modeling

The DCM focused on how reward-induced response inhibition (HIC vs. LIC) related to the incongruent target was implemented through the connectivities in the brain. Different models of functional architecture and effective connectivity were compared using DCM10 implemented in SPM8. Here we used bilinear DCM, which consists of 3 different sets of parameters (Friston et al. 2003): 1) the “intrinsic” connectivity representing the latent connectivity between brain regions irrespective of experimental conditions; 2) the “modulatory” connectivity representing the influence of experimental conditions on the intrinsic connectivity; and 3) “input” representing the driving influence on brain regions by the experimental conditions.

We extracted activation time courses (eigenvariate) from a sphere with a 3-mm radius centered on the group peak coordinates of pre-SMA, right IFC, right STN, and right caudate revealed by the contrast of “HIC > LIC” in each participant. These areas, as well as the structural and functional connection between them, were also well-documented for controlling response inhibition (Madsen et al. 2010; Coxon et al. 2012; Swann et al. 2012). The intrinsic connectivities between each 2 areas were constructed according to previous models that based on effective connectivity (Jahfari et al. 2011; Herz et al. 2014): unilateral connectivity from the frontal pathway (rIFC, pre-SMA) to rSTN and rCaudate, and bilateral connectivity between rIFC and pre-SMA. We constructed 7 models sharing the same intrinsic connectivity pattern, but differed in the structure of the modulatory connectivity exerted by reward (HIC vs. LIC). Figure 6A illustrates the structure of the modulatory connectivity in the 7 single models. In all of the models compared here, pre-SMA received the model input because previous studies on response inhibition revealed that the activity in pre-SMA precedes the activity in rIFC (Neubert et al. 2010; Swann et al. 2012), and because it has been suggested that pre-SMA projects information to and recruits other areas in the frontobasal ganglia network to inhibit the inappropriate response (Forstmann et al. 2008; Hikosaka and Isoda 2010; Neubert et al. 2010; Swann et al. 2012).

Based on our hypothesis, the potential reward modulation could be exerted on 1) all of the connections between each 2 areas (a full model, model 1); 2) the connection within pre-SMA and rIFC (the frontal pathway), and the connection from the frontal areas to the basal ganglia areas (the frontobasal ganglia pathway) (models 2 and 3); 3) the connection from the frontal areas to the basal ganglia areas (frontal-basal ganglia pathway only, models 4, 5, and 6); and 4) only the connection within the frontal areas (frontal pathway only, model 7).

These models were then compared using the Bayesian Model Selection (BMS), which uses a Bayesian framework to compute the “model evidence” for each model, representing the trade-off between model simplicity and model fitness (Penny et al. 2004). Here, BMS was implemented using a random-effect analysis (i.e., assuming that the model structure may vary across participants) that is robust to the presence of outliers (Stephan et al. 2009). Based on the estimated model evidence for each model, the random effect BMS calculates the exceedance probability, that is, the probability of a model being more likely than any other model. Model parameters were estimated from the model with the highest exceedance probability. The median of each model parameter was compared with the hypothesized median 0 using Wilcoxon signed rank test because some of the model parameters did not follow a normal distribution. Multiple comparisons were corrected with the Bonferroni method.

The hypothesis tested by our DCM analysis was which pathway(s) was modulated by reward in regulating response inhibition. For this purpose, we constructed the model space based on a well-established model of response inhibition, which assumes a unidirectional pathway from the frontal network to the basal ganglia (Jahfari et al. 2011; Herz et al. 2014). A relevant question here might be how reward information is received and projected to the frontal areas in modulating response inhibition. One might argue that, given its important role in reward processing (Cromwell and Schultz 2003), the caudate could be involved in this process. However, previous studies have shown that the anterior insula (AI) and the ventral striatum (VS), 2 areas in the reward circuit (Haber and Knutson 2010), and the connectivity between AI and VS, are critical in regulating the attentional control for reward-associated stimuli (Rothkirch et al. 2014; Wang et al. 2015). Considering the ongoing debate, we did not include additional models in our DCM analysis to test how reward information is received and projected to the frontal areas. However, we did explore whether the DCM results reported here were biased by the lack of a pathway from right caudate to the prefrontal network. We compared models which include unidirectional pathway from right caudate to the frontal network and models which include bidirectional connectivity (Supplementary Fig. S1) with the 7 models reported here. The model comparison showed that including models with the connectivity from right caudate to the frontal network did not change the DCM results here (Supplementary Fig. S1).

Results

Behavioural Data

Experiment 1

For Experiment 1A, a 2 (Reward: high vs. low) \times 2 (Spatial congruency; congruent vs. incongruent) repeated-measures ANOVA revealed that RTs were faster for the high-reward letters (394 ms) than for the low-reward letters (415 ms), $F(1, 19) = 14.67$, $P = 0.001$, $\eta_p^2 = 0.436$, and that RTs were faster in the congruent conditions (392 ms) than in the incongruent conditions (417 ms), $F(1, 19) = 92.75$, $P < 0.001$, $\eta_p^2 = 0.830$, that is, the typical Simon effect (Fig. 2A, left panel). Moreover, an interaction between reward and spatial congruency was observed, $F(1, 19) = 6.26$, $P = 0.022$, $\eta_p^2 = 0.248$, with the Simon effect, that is, RTs in the incongruent condition minus RTs in the congruent condition, being larger for the high-reward targets (33 ms) than for the low-reward targets (18 ms) (Fig. 2A, left panel). Analyses on error rates revealed only a main effect of congruency, with more errors in the incongruent conditions (7.2%) than the congruent conditions (3.6%), $F(1, 19) = 31.12$, $P < 0.001$, $\eta_p^2 = 0.621$, whereas neither the main effect of reward, $F < 1$, nor the interaction, $F(1, 19) = 1.31$, $P = 0.267$, reached significance (Fig. 2A, middle panel).

For the distributional analysis, Simon effects are plotted as a function of the mean bin RT in Figure 2A (right panel). Paired t tests showed that the intercept (i.e., the parameter a) in the high-reward condition (34 ms) was larger than the intercept in the low-reward condition (22 ms), $t(19) = 2.09$, $P = 0.050$, indicating a larger Simon effect in the high-reward condition even after the effect of response speed had been regressed out. One-sample t tests showed that the slope (i.e., the parameter b) in the low-reward condition (-0.11) was lower than zero, $t(19) = 2.98$, $P = 0.008$, indicating that Simon effect decreased as a function of response speed. By contrast, the slope in the high-reward condition (0.10) showed a trend of being higher than zero, $t(19) = 2.03$, $P = 0.057$ (Fig. 2A, right panel). In addition, the

slope in the high-reward condition was higher than the slope in the low-reward condition, $t(19) = 3.35$, $P = 0.003$.

For Experiment 1B, the ANOVA on RTs showed a main effect of reward, with faster RTs for the high-reward digits (416 ms) than for the low-reward digits (441 ms), $F(1, 19) = 26.18$, $P < 0.001$, $\eta_p^2 = 0.579$. The main effect of congruency was significant, with faster RTs in the congruent conditions (422 ms) than in the incongruent conditions (435 ms), $F(1, 19) = 19.04$, $P < 0.001$, $\eta_p^2 = 0.501$. There was also an interaction between reward and congruency, $F(1, 19) = 11.95$, $P = 0.003$, $\eta_p^2 = 0.386$, with a larger Simon effect for the high-reward targets (20 ms) than for the low-reward targets (6 ms) (Fig. 2B, left panel). Analyses on error rates revealed only a trend of congruency effect, with more errors in the incongruent conditions (8.6%) than in the congruent conditions (6.1%), $F(1, 19) = 4.28$, $P = 0.052$, $\eta_p^2 = 0.184$, whereas neither the main effect of reward, $F(1, 19) = 1.33$, $P = 0.264$, nor the interaction, $F < 1$, reached significance (Fig. 2B, middle panel).

A similar distributional analysis on Simon effect was carried out for Experiment 1B. Paired t tests on the parameter estimates of the model fitting showed a pattern of results similar to Experiment 1A. Specifically, the intercept in the high-reward condition (22 ms) was larger than the intercept in the low-reward condition (9 ms), $t(19) = 2.32$, $P = 0.032$, indicating a larger Simon effect in the high-reward condition even after the effect of response speed had been regressed out. One-sample t tests showed that the slope in the low-reward condition (-0.17) was lower than zero, $t(19) = 3.71$, $P = 0.001$, indicating that the Simon effect decreased as a function of response speed. By contrast, the slope in the high-reward condition (-0.06) did not differ from zero, $t(19) = 1.16$, $P = 0.260$ (Fig. 2A, right panel). In addition, the slope in the high-reward condition showed a trend of being less negative than the slope in the low-reward condition, $t(19) = 1.98$, $P = 0.062$.

Experiment 2 (EEG Experiment)

The 2 \times 2 ANOVA on RTs showed a main effect of reward, $F(1, 23) = 66.14$, $P < 0.001$, $\eta_p^2 = 0.742$, with faster responses to the high-reward targets (389 ms) than to the low-reward targets (426 ms), and a main effect of spatial congruency, $F(1, 23) = 13.01$, $P = 0.001$, $\eta_p^2 = 0.361$, with faster responses to the congruent targets (402 ms) than to the incongruent targets (413 ms). The interaction between reward and congruency was also significant, $F(1, 23) = 13.52$, $P = 0.001$, $\eta_p^2 = 0.370$, with a larger Simon effect for the high-reward targets (20 ms) than for the low-reward targets (2 ms) (Fig. 2C, left panel). Analyses on error rates showed a main effect of reward, with fewer errors in the high-reward conditions (5.2%) than in the low-reward conditions (6.0%), $F(1, 23) = 6.81$, $P = 0.016$, $\eta_p^2 = 0.228$. There was no main effect of spatial congruency, $F < 1$, but an interaction between reward and congruency, $F(1, 23) = 5.71$, $P = 0.025$, $\eta_p^2 = 0.199$. Further paired- t tests revealed that the Simon effect in terms of error rate was observed for the high-reward targets (1.7%), $t(23) = 2.46$, $P = 0.022$, but not for the low-reward targets (-1.1%), $t < 1$ (Fig. 2C, middle panel).

The distributional analysis and model fitting on RTs showed that the intercept in the high-reward condition (25 ms) was larger than the intercept in the low-reward condition (10 ms), $t(23) = 2.68$, $P = 0.013$, indicating an increased Simon effect in the high-reward condition even after the effect of response speed had been regressed out. The slope in the low-reward condition (-0.21) was smaller than zero, $t(23) = 5.61$, $P < 0.001$, indicating a decreased Simon effect as a function of response speed, whereas

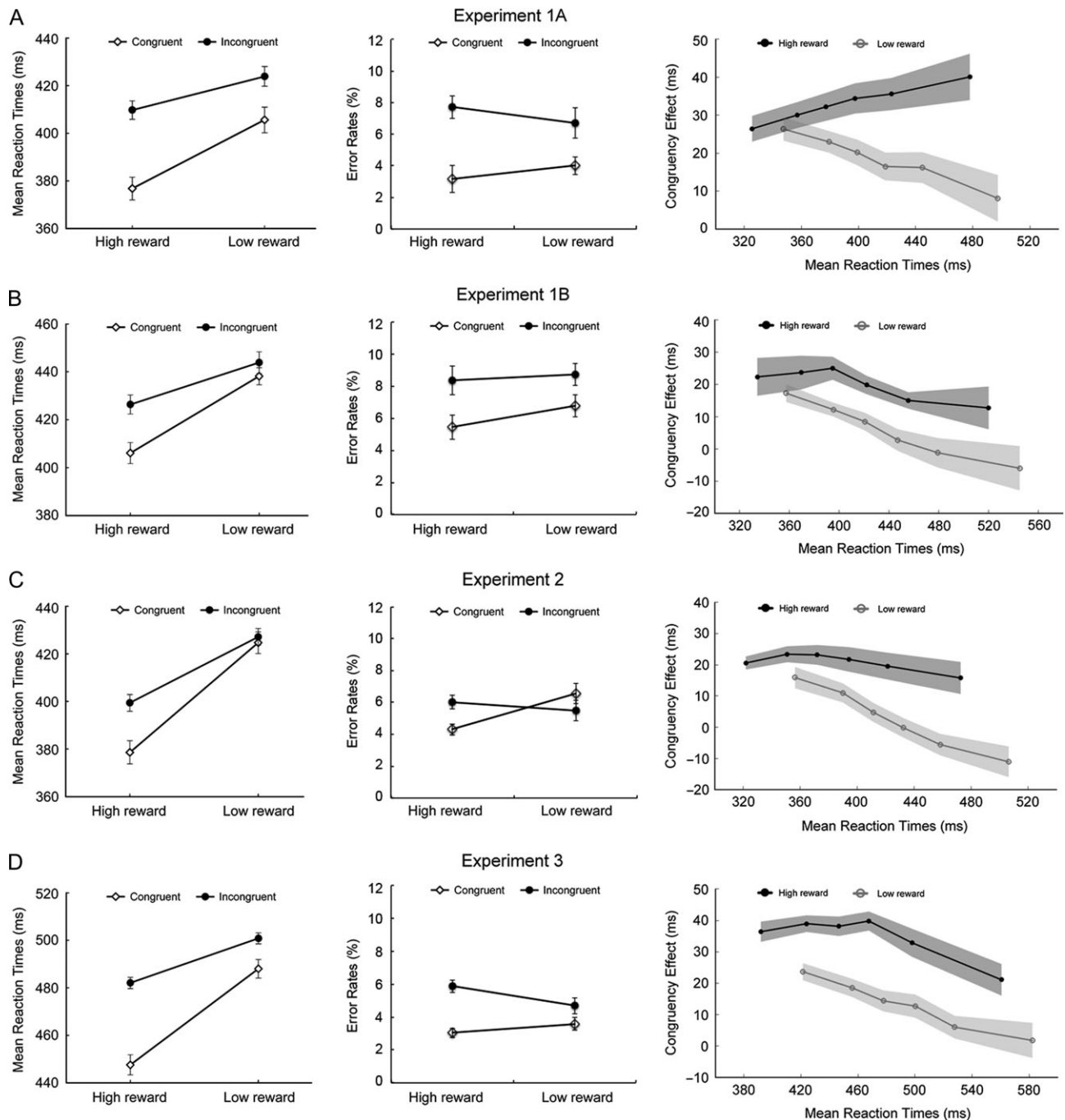


Figure 2. Behavioral results of Experiments 1A (A), 1B (B), 2 (C), and 3 (D). *Left panel:* mean reaction times (RT) are shown as a function of reward (high vs. low) and spatial congruency (congruent vs. incongruent). *Middle panel:* error rates are shown as shown as a function of reward and spatial congruency. *Right panel:* The congruency effects were calculated as the difference in RTs between incongruent trials and congruent trials, and are shown as a function of the mean RT in different bins for high-reward and low-reward conditions. Error bars and shades denote within-subject standard errors (Cousineau 2005).

the slope in the high-reward condition (-0.00) did not differ from zero, $t < 1$, indicating equivalent Simon effects across different response speeds (Fig. 2C, right panel). In addition, the slope in the high-reward condition was higher than the slope in the low-reward condition, $t(23) = 3.28$, $P = 0.003$.

Experiment 3 (fMRI Experiment)

The ANOVA on RTs showed a main effect of reward, $F(1, 23) = 76.68$, $P < 0.001$, $\eta_p^2 = 0.769$, with faster responses to the high-

reward targets (465 ms) than to the low-reward targets (495 ms), and a main effect of spatial congruency, $F(1,23) = 111.90$, $P < 0.001$, $\eta_p^2 = 0.830$, with faster responses to the congruent targets (468 ms) than to the incongruent targets (492 ms). There was also an interaction between reward and congruency, $F(1, 23) = 15.75$, $P = 0.001$, $\eta_p^2 = 0.406$, with a larger Simon effect for the high-reward targets (35 ms) than for the low-reward targets (13 ms) (Fig. 2D, left panel). Analyses on error rates revealed only a main effect of spatial congruency, $F(1, 23) = 18.11$, $P <$

0.001, $\eta_p^2 = 0.441$, whereas neither the main effect of reward, $F < 1$, nor the interaction, $F(1, 23) = 2.92$, $P = 0.101$, reached statistical significance (Fig. 2D, middle panel).

For the distributional analysis and the model fitting, the intercept in the high-reward condition (37 ms) was larger than the intercept in the low-reward condition (18 ms), $t(23) = 3.73$, $P = 0.001$, indicating an increased Simon effect in the high-reward condition even after the effect of response speed had been regressed out. The slope in the low-reward condition (-0.16) was smaller than zero, $t(23) = 4.45$, $P < 0.001$, indicating a decreased Simon effect as a function of response speed, whereas the slope in the high-reward condition (-0.02) did not differ from zero, $t < 1$, indicating equivalent Simon effects across different response speeds (Fig. 2D, right panel). In addition, the slope in the high-reward condition was higher than the slope in the low-reward condition, $t(23) = 2.50$, $P = 0.020$.

EEG Data

ERPs

Figure 3A shows the averaged waveforms of the stimulus-locked LRP. For the early time window, ANOVA revealed a significant main effect of congruency, $F(1, 23) = 7.34$, $P = 0.013$,

$\eta_p^2 = 0.242$, with negative LRP responses to the congruent trials and positive LRP responses to the incongruent trials. The main effect of reward was not significant, $F < 1$. However, there was a significant interaction between reward and congruency, $F(1, 23) = 6.65$, $P = 0.017$, $\eta_p^2 = 0.224$, driven by a larger amplitude difference between the high reward incongruent (HIC) trials (0.67 μV) and high reward congruent (HC) trials ($-1.41 \mu\text{V}$) than the difference between the low reward incongruent (LIC) trials (0.98 μV) and the low reward congruent (LC) trials ($-0.53 \mu\text{V}$). Moreover, at the individual level, the amplitude difference modulated by reward showed a correlation with RT difference modulated by reward, $r = 0.569$, $P = 0.004$. For the late time window, no significant effect was revealed, all P s > 0.2 .

Figure 3B shows the averaged waveforms of the response-locked LRP. For the early time window, ANOVA revealed a significant main effect of congruency $F(1, 23) = 6.80$, $P = 0.016$, $\eta_p^2 = 0.228$, with more negative LRP in the congruent conditions than in incongruent conditions. The main effect of reward was not significant, $F < 1$. The interaction between reward and congruency was significant, $F(1, 23) = 18.29$, $P < 0.001$, $\eta_p^2 = 0.443$, which was driven by a larger amplitude difference between HIC trials (0.97 μV) and HC trials ($-0.81 \mu\text{V}$) than the difference between LIC trials (0.78 μV) and LC trials (0.36 μV). There was

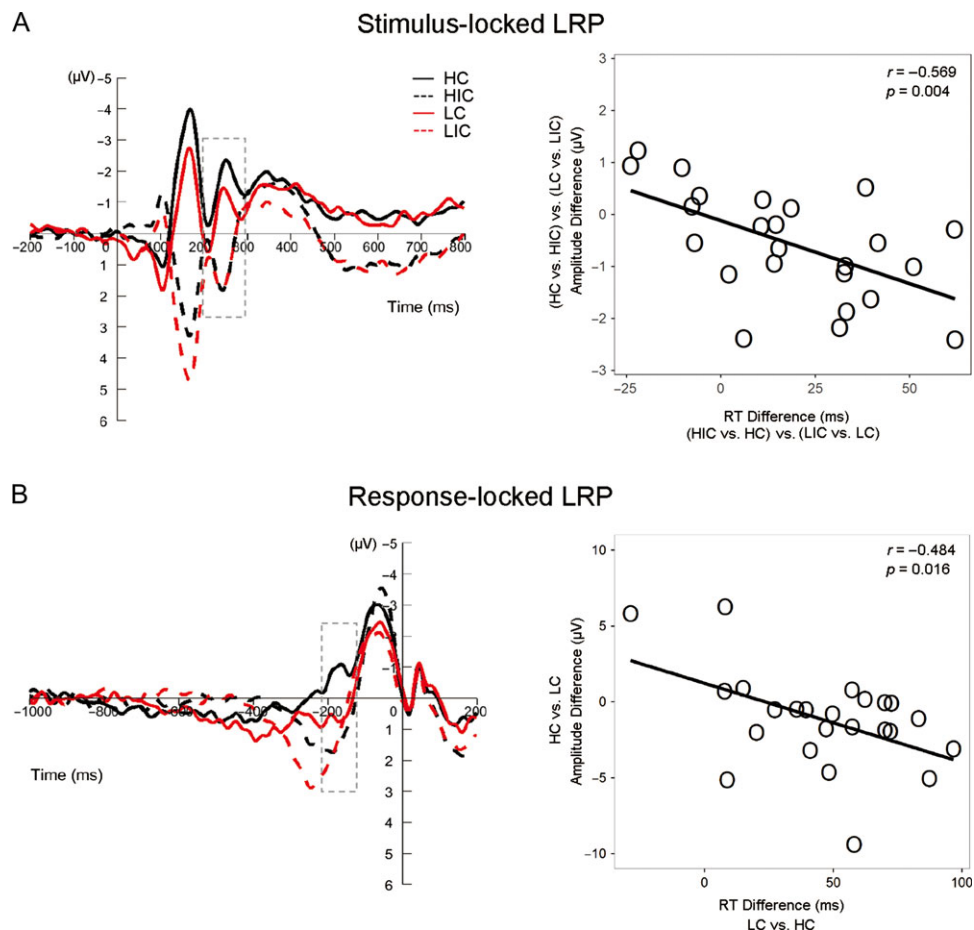


Figure 3. ERP results of Experiment 2. The ERP responses were obtained by subtracting the signals at the ipsilateral motor cortex (C3/C4) from the signals at the contralateral motor cortex (C4/C3) of the response hand. (A) The ERP responses locked to the stimulus onset in the 4 experimental conditions (left panel). Scatter plots (with best-fitting regression lines) illustrate the difference of the LRP amplitude in the early time window between HIC and LIC conditions as a function of the RT (right panel). (B) The ERP responses locked to the response onset. Scatter plots (with best-fitting regression lines) illustrates the difference of the LRP amplitude in the early window between HIC and LIC conditions as a function of the RT (right panel). Dashed lines indicate the early time windows during which the LRP amplitudes showed an interaction between reward and congruency.

also a trend for a difference in LRP amplitude between high and low reward congruent trials, $t(23) = -1.77$, $P = 0.09$, whereas there was no difference in LRP amplitude between high and low reward incongruent trials, $t < 1$. Moreover, at the individual level, the amplitude difference between high and low reward congruent conditions showed a correlation with RT difference between these 2 conditions, $r = 0.484$, $P = 0.016$. For the late time window, no significant effects were found, all P s > 0.2 . Here the reward modulation on LRP manifested mainly for the congruent trials. This might be related to the fact that both the reward-induced response activation and inhibition, which might counteract with each other, were involved for incongruent trials, whereas only the reward-induced response activation was involved for congruent trials.

Frontal Theta Oscillations

The topographical distribution of theta band oscillations is shown in Figure 4. The permutation tests found no significant clusters for the low-reward conditions (P s = 1, Fig. 4B). However, Fz, F1, F2, F3, F4, FCz, FC1, FC2, FC3, FC4, FC6, Cz, C1, C2, C4, C5, and C6 were grouped as a significant cluster for the

high-reward conditions, with the frequency ranging from 6 to 8 Hz and the time interval ranging from 180 to 570 ms postonset (cluster statistics = 2739.5, $P = 0.006$, Fig. 4A), suggesting that frontal theta oscillations were stronger in the HIC condition (97.7% in power change averaged across the whole cluster) than in the HC condition (58.1% power change). As shown in Figure 4, the strongest theta activity was located at FCz. For the interaction between reward and congruency, Fz, F1, F2, F3, F4, F5, F6, FCz, FC1, FC2, FC3, Cz, C1, C2, C3 were grouped as a significant cluster with frequency ranging from 6 to 8 Hz and time interval ranging from 370 to 730 ms (cluster statistic = 1273.9, $P = 0.045$, Fig. 4C).

fMRI Data

Region of Interest (ROI) Analysis in M1

For the contralateral M1, the ANOVA showed only a main effect of reward, $F(1, 23) = 5.77$, $P = 0.025$, $\eta_p^2 = 0.201$, but no main effect of congruency, or interaction, both $F < 1$, indicating enhanced motor activation by reward for the correct response hand (Fig. 5A). The reward-facilitated behavioral response (RT

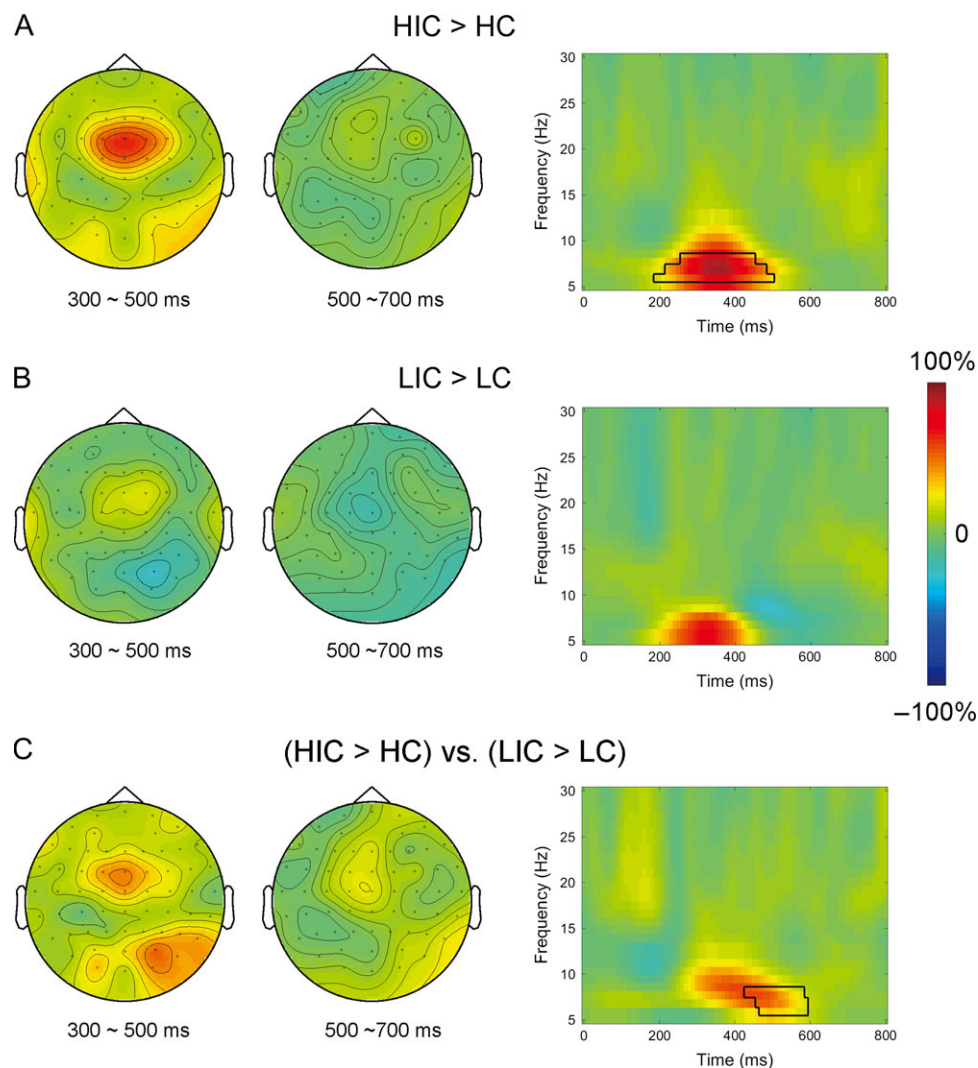


Figure 4. Results of time frequency analysis revealed by “HIC > HC” (A), “LIC > LC” (B), and the interaction “HIC > HC” vs. “LIC > LC” (C). Left panel: topographical distribution of the power change in theta oscillation (300–700 ms poststimulus onset). Right panel: the power change at FCz as a function of frequency and time. The region marked by the black line indicates the power change that reached significance after the correction for multiple comparisons.

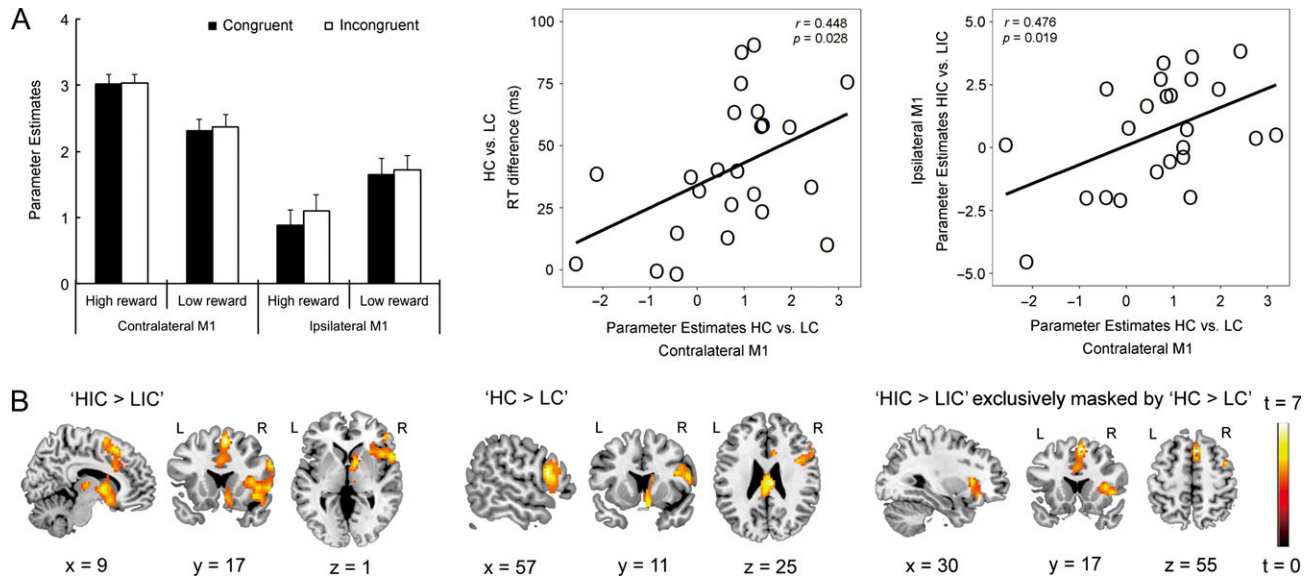


Figure 5. (A) Parameter estimates extracted from the peak voxel in M1 that contralateral to the correct response hand and the peak voxel in M1 that ipsilateral to the correct response hand are shown as the function of the 4 experimental conditions (left panel). The scatter plot (with the best-fitting regression line) illustrates the RT difference between LC and HC conditions as a function of the reward-induced response activation strength in contralateral M1 (middle panel). The scatter plot (with the best-fitting regression line) illustrates the reward-induced response inhibition strength in ipsilateral M1 as a function of the reward-induced response activation strength in contralateral M1 (right panel). (B) Brain areas revealed by the contrasts: “HIC > LIC” (left panel), “HC > LC” (middle panel), and “HIC > LIC” exclusively masked by “HC > LC” (right panel). Statistical parametric map is shown at the threshold of $P < 0.001$ FWE-corrected at cluster level, $P < 0.001$ uncorrected at voxel level.

difference between the HC and LC conditions) correlated with the reward-enhanced motor activation in the contralateral M1, $r = 0.448$, $P = 0.028$ (Fig. 5B, left panel). For the ipsilateral M1, there was a main effect of congruency, $F(1, 23) = 6.34$, $P = 0.019$, $\eta_p^2 = 0.216$, indicating that incongruent trials induced stronger activity in the contralateral motor cortex than congruent trials. However, the main effect of reward, $F(1, 23) = 2.32$, $P = 0.141$ and the interaction, $F(1, 23) = 2.29$, $P = 0.144$, did not reach significance. The lack of a significant interaction here might be due to the entangled reward-induced response activation and inhibition for the HIC condition (vs. LIC condition), the separation of which suffered from the poor temporal resolution of fMRI. Critically, the reward-induced inhibition strength in the ipsilateral M1 showed a correlation with the reward-induced activation strength in the contralateral M1, $r = 0.476$, $P = 0.019$ (Fig. 5B, right panel), suggesting that the individual participants' reward-induced inhibition strength was dependent on the reward-induced activation strength.

Whole-Brain Contrasts

We conducted the contrast “HIC > LIC” across the whole brain to identify areas involved in coping with the inappropriate response activation that was enhanced by reward. The contrast revealed a frontobasal ganglia network including pre-SMA, right IFC, right subthalamus where the peak voxel was localized in STN, and dorsal striatum where the peak voxel was localized in right caudate (Fig. 5B, left panel; Table 1). The reverse contrast “LIC > HIC” did not reveal any activated areas. The contrast “HC > LC” revealed the activation of right nucleus accumbens (NAcc), right IFC and posterior cingulate cortex (Fig. 5B, middle panel; Table 1). The reverse contrast “LC > HC” did not reveal any activated areas. More importantly, pre-SMA and right IFC could still be observed when the contrast “HIC > LIC” was exclusively masked by the areas activated by the contrast “HC > LC” (Fig. 5B, right panel; Table 1), suggesting the role of

pre-SMA and right IFC in inhibiting the inappropriate response activation was enhanced by reward, rather than playing an augmented role in the reward-enhanced response activation.

Dynamic Causal Modeling

Figure 6A shows the exceedance probabilities derived from the Bayesian model comparison on the 7 models. The winning model was the one where only the intrinsic connectivities within the frontal areas were modulated by reward (i.e., the frontal pathway). The model parameters estimated based on the winning model are depicted in Figure 6B. Importantly for the modulatory connectivities, the HIC, but not the LIC, condition significantly enhanced the connectivity from pre-SMA to rIFC. There was no modulatory effect on the connectivity from rIFC to pre-SMA. These results suggest that the high-reward significantly enhanced the connectivity from pre-SMA to rIFC, whereas the low-reward failed to reliably alter the connectivity.

Discussion

In this study, we showed that reward can enhance automatic response activation in the motor cortex, which is overcome by active response inhibition when it conflicts with the correct response. The dynamic interactions between MFC and rIFC plays a causal role in controlling reward-induced response inhibition, suggesting an important role of the frontal cortex in motivating cognitive control (Kouneiher et al. 2009).

Reward-Induced Response Activation in the Motor Cortex

According to the dual-mechanism model, the lateral target triggers automatic response activation at the spatially corresponding hand, which causes facilitation when this activation is congruent with the task-required hand whereas it causes

Table 1 Brain areas revealed by the contrasts: “HIC > LIC,” “HC > LC,” and “HIC > LIC” exclusively masked by “HC > LC.” Coordinates (x, y, z) correspond to MNI space

Region	Hemisphere	MNI coordinates of peak voxel			t Value	Cluster size
		x	y	z		
“HIC > LIC”						
Pre-SMA/dACC	L/R	6	17	55	7.30	336
IFC	R	57	14	1	6.19	792
Caudate	R	9	5	4	6.06	122
STN	R	6	-16	7	5.61	37
“HC > LC”						
IFC	R	57	14	16	6.82	167
PCC	L/R	6	-22	25	6.78	229
NAcc	R	6	11	-17	5.48	140
“HIC > LIC” exclusively masked by “HC > LC”						
Pre-SMA/dACC	L/R	6	17	55	7.30	322
IFC	R	30	20	7	6.13	386

Notes: dACC = dorsal anterior cingulate cortex; IFC = inferior frontal cortex; NAcc = nucleus accumbens; PCC = posterior cingulate cortex; pre-SMA = presupplementary motor area; STN = subthalamic nucleus.

conflict when this activation is opposite to the task-required hand (De Jong et al. 1994; Ridderinkhof 2002). From this perspective, increased conflict for the high-reward targets in our data suggests an enhanced response activation by reward.

One alternative account could be that high-reward (vs. low-reward) targets possess higher salience (Berridge and Robinson 1998; Wang et al. 2015), which could facilitate the response to the target. Given that the Simon effect decreases as a function of response speed, the larger Simon effect in the high-reward condition relative to the low-reward condition could have appeared as a by-product of the reward-enhanced response speed. This account, however, seems to be inconsistent with the increased conflict by high-reward target after the response speed had statistically been regressed out. More importantly, in contrast to a linear decrease of response conflict for low-reward targets, which confirmed the transient nature of response activation (De Jong et al. 1994), the conflict induced by high-reward targets did not decrease with increasing RTs to the same extent as the conflict induced by low-reward targets, suggesting a sustained response activation. Taken together, our behavioral results suggest that the reward-enhanced conflict cannot be simply attributed to the facilitated responses to the high-reward targets.

The reward-induced response activation in the Simon task echoes previous studies using other cognitive control tasks. For example, Freeman et al. (2014, 2016) showed that a NoGo stimulus that has been predictive of reward induces more erroneous responses, compared with a NoGo stimulus that has not been predictive of reward. In a Stroop task, Krebs et al. (2010, 2011) found slower responses to an incongruent word when the word meaning is related to a reward-associated color. The consistent results from various tasks point towards a common prepotent response activation modulated by reward.

Here we provide direct neural evidence for such response activation with the BOLD signal in the motor cortex, and the ERP component LRP, which is mainly generated within primary motor cortex (Leuthold and Jentsch 2002). A negative LRP indicates response activation at the correct hand while a positive LRP indicates response activation at the incorrect hand (van Schie et al. 2004; Leuthold 2011). The ERP results showed that the congruent targets induce negative LRP, whereas incongruent targets induce positive LRP, which turns to be negative in a

later epoch, replicating the response activation pattern over the motor cortex in previous studies (Sommer et al. 1993; Valle-Inclan and Redondo 1998). In an extension, our results showed that such response activation is modulated by reward. Specifically, relative to the low-reward targets, the high-reward targets induce a stronger LRP and greater BOLD signals in M1, and these reward-triggered modulations on the motor activity could predict the reward-triggered modulation in RTs, suggesting enhanced motor activation by reward-associated stimuli.

Reward-Enhanced Response Inhibition in the Frontal Pathway

In the human brain, cognitive control is closely related to MFC (Ridderinkhof et al. 2004; Boehler et al. 2010; Duque et al. 2013). This notion gains support from EEG evidence showing theta-band oscillations along the midfrontal channels (Cohen and Cavanagh 2011; Nigbur et al. 2012) and brain imaging and stimulation evidence showing a crucial role of pre-SMA (Duque et al. 2013; Rae et al. 2014) during response inhibition. Along these lines, our results further revealed that response inhibition by MFC could be modulated by reward. In our EEG experiment, midfrontal theta oscillations were more recruited to resolve the response conflict in the high-reward conditions than in the low-reward condition. Similarly, in our fMRI experiment, pre-SMA exhibited higher BOLD signals in the HIC condition than in the LIC condition. These results are consistent with Krebs et al. (2011) who showed an increased BOLD signal in pre-SMA when the incongruent meaning of the Stroop word is related to reward. The converging evidence suggests that MFC is responsible for coping with the inappropriate response activation reinforced by reward.

Another key brain site involved in inhibitory control is rIFC (Aron et al. 2007; Forstmann et al. 2008; Boehler et al. 2010), which is considered as a brake to implement inhibitory control (Aron et al. 2014). In a stop-signal task, Padmala and Pessoa (2010) showed that rIFC is more active during response inhibition in a reward context, compared with a no-reward context. Similarly in the present study, boosted activity in rIFC was also observed when the incongruent targets was associated with high-reward, suggesting that the involvement of rIFC in response inhibition is modulated by reward. Moreover, our

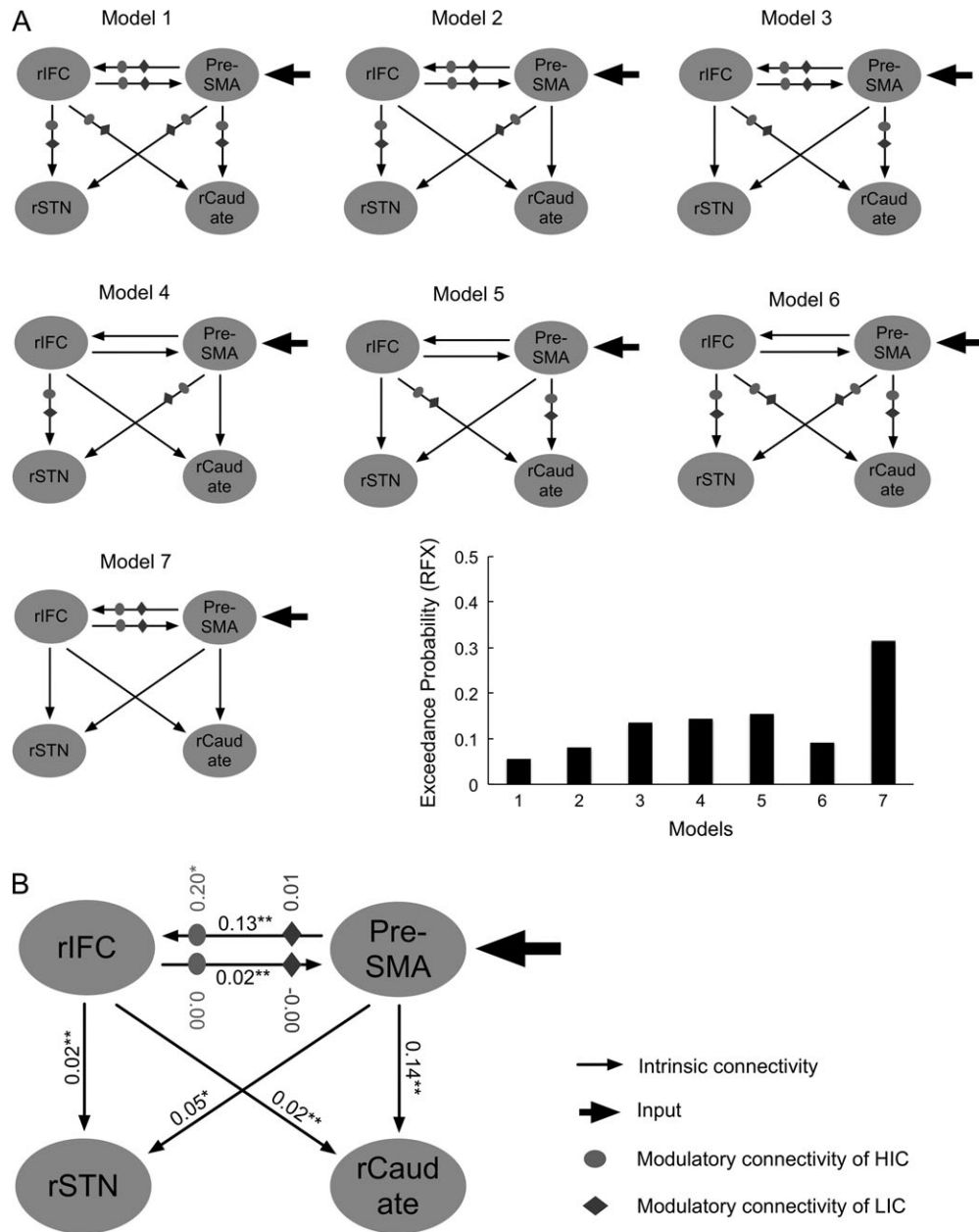


Figure 6. The dynamic causal modeling (DCM) for pre-SMA, rIFC, rSTN, and rCaudate. (A) The structure of 7 models which differed in the specific pathway(s) that modulated by reward (HIC vs. LIC), and the exceedance probabilities of the 7 models. (B) The estimated DCM parameters of the winning model (* $P < 0.05$, ** $P < 0.01$, with Bonferroni correction for multiple comparisons).

DCM results showed that the functional connectivity from pre-SMA to rIFC was strengthened in the HIC condition, where there was a stronger need for response inhibition. This is in line with a previous study showing increased effective connectivity between pre-SMA and right lateral prefrontal cortex when cognitive control is implemented in a reward context (Kouneiher et al. 2009). As an extension, our DCM results revealed a causal role of the connectivity from pre-SMA to rIFC in implementing reward-enhanced response inhibition, suggesting the critical role of the frontal pathway in motivating response inhibition. The convergent EEG and fMRI-DCM evidence in the present study is in agreement with the notion that MFC computes the benefit-cost of control and regulates cognitive resources in the lateral prefrontal cortex, which in turn

governs the inhibition of inappropriate responses (Kouneiher et al. 2009; Rushworth et al. 2004; Shenhav et al. 2013).

The critical role of the frontal pathway in implementing reward-enhanced response control in the present study seemed at odds with the frontosubthalamic connectivity in Herz et al. (2014). Such different neural mechanisms, however, may point to the dual mechanisms of cognitive control, which suggest proactive control and reactive control as 2 distinct manners of control (Braver 2012). According to this framework, the task goal is actively maintained before the occurrence of cognitively demanding events in proactive control, whereas the adjustment is mobilized in a “late correction” manner in reactive control (Braver 2012). In Herz et al. (2014), trials with the prospect of reward gain were blocked in the way that conflict

control could be motivated and actively maintained during a block. By contrast in the present study, given that the reward information was unpredictable until the onset of the target in each trial, conflict control was thus recruited after detecting the incompatible response tendencies. As a result of the task context at hand, it is likely that proactive control was dominant in the former case whereas reactive control was dominant in the latter case. Future studies are therefore needed to elucidate whether the neural mechanism (e.g., frontal-basal ganglia pathway vs. frontal pathway) underlying the reward modulation on cognitive control is critically dependent on the dominant control mode (proactive vs. reactive).

The 2-Stage Model of Reward-Induced Response Activation and Inhibition

Based on both behavioral and physiological evidence, Freeman et al. proposed a 2-stage processing model to explain the reward-induced response activation and inhibition (Freeman et al. 2014; Freeman and Aron 2016). In the first stage, reward-related stimuli enhance early response activation. This enhanced response activation by reward results in both faster RTs for Go stimuli and more errors for NoGo stimuli, accompanied by enhanced effector-muscle activity. In the second stage, response inhibition needs to overcome the inappropriate response activation for NoGo stimuli. The inhibition strength, as measured by muscle activity, crucially depends on the activation strength. Specifically, reward-related stimuli recruit stronger response inhibition than reward-unrelated stimuli, and the inhibition strength could be individually predicted by the activation strength. In the current study, consistent with the first stage of the model, we found an early reward-enhanced response activation in the motor cortex. This enhanced response tendency could facilitate the response when it is congruent with the correct response hand, but caused stronger conflict when it is incongruent with the correct response hand, thereby requiring stronger inhibitory control to overcome the enhanced, inappropriate response tendency. Correspondingly, we found frontal theta oscillations which were accompanied by the attenuation of the reward-enhanced response activation in the late time window, and the activation of the frontal-basal ganglia network of response inhibition. Moreover, the reward-modulated inhibition strength in the task-irrelevant M1 crucially depends on the reward-induced activation strength in the task-relevant M1. These neural activities accord well with the reward-modulated inhibition in the second stage of the model. As such, our results reveal the neural correlates of the 2 processing stages and the corresponding neural dynamics of the reward-induced response activation and inhibition.

Despite the apparently similar patterns of reward-enhanced response activation and the corresponding response inhibition to overcome the inappropriate response activation, different mechanisms may be involved in the response inhibition outlined in the 2-stage model and the response inhibition observed in the current study. In previous studies (Freeman et al. 2014; Freeman and Aron 2016), inhibiting/withholding the enhanced response tendency to the reward-associated stimuli is accomplished with the aim of achieving the task goal at hand, because reward is only expected in Go trials but not in NoGo trials. By contrast in the current study, response inhibition was not only recruited to achieve the task goal, but also motivated to gain the upcoming reward, which underlies the approach-approach conflict between 2 desired responses in a real-world

situation. Taken together, the similar patterns in the 2 lines of studies point to a common 2-stage model of reward-enhanced response activation and the corresponding response inhibition, irrespective of the particular goal of the response inhibition.

The current findings concerning the interaction between reward and response activation/inhibition may help to understand the neural dynamics underlying self-control disorders. Response inhibition is a central component of cognitive control (Logan 1994; Ridderinkhof et al. 2011; Bari and Robbins 2013; Aron et al. 2014). The dysfunction of response inhibition characterizes self-control disorders such as attention deficit/hyperactivity disorder (ADHD), addiction and obsessive compulsive disorder (OCD) (Chambers et al. 2009). Moreover, patients with such maladaptive behaviors often show deficits in responding to reward, accompanied by dysfunctions of the dopamine reward pathway (Figeo et al. 2011; Volkow, et al. 2011). It is possible that the parallel deficits in response inhibition and reward processing interactively contribute to the manifestation of self-control disorders in these patients.

In summary, the present study demonstrates that reward-associated stimuli promote early response activation, which asks for a top-down response inhibition, through the dynamic interaction between MFC and rIFC, to overcome the enhanced, inappropriate response activation when it is incongruent with the current goal, delaying behavioral responses. Our findings provide a dynamic neural model for the reward-induced response inhibition and can advance our understanding of the neural communication between reward and cognitive control in generating adaptive behaviors.

Supplementary Material

Supplementary material is available at *Cerebral Cortex* online.

Funding

National Basic Research Program of China (973 Program: 2015CB856400) and the Natural Science Foundation of China (Grant 31630034) to Xiaolin Zhou, an advanced grant awarded to Jan Theeuwes by the European Research Council (ERC-2012-AdG-323413), and Grant 636116 awarded to Ruth M. Krebs by the European Research Council (ERC) under the Horizon 2020 framework.

Notes

We thank Mr Kaiwen Jiang for conducting pilot experiments, and Miss Xiaoxue Gao for assisting fMRI data collection. *Conflict of Interest*: None declared.

References

- Aron AR, Berens TE, Smith S, Frank MJ, Poldrack RA. 2007. Triangulating a cognitive control network using diffusion-weighted magnetic resonance imaging (MRI) and functional MRI. *J Neurosci.* 27(14):3743–3752.
- Aron AR, Herz DM, Brown P, Forstmann BU, Zaghoul K. 2016. Frontosubthalamic circuits for control of action and cognition. *J Neurosci.* 36(45):11489–11495.
- Aron AR, Poldrack RA. 2006. Cortical and subcortical contributions to Stop signal response inhibition: role of the subthalamic nucleus. *J Neurosci.* 26(9):2424–2433.
- Aron AR, Robbins TW, Poldrack RA. 2014. Inhibition and the right inferior frontal cortex: one decade on. *Trends Cogn Sci.* 18(4):177–185.

- Awh E, Belopolsky AV, Theeuwes J. 2012. Top-down versus bottom-up attentional control: a failed theoretical dichotomy. *Trends Cogn Sci.* 16(8):437–443.
- Bari A, Robbins TW. 2013. Inhibition and impulsivity: behavioral and neural basis of response control. *Prog Neurobiol.* 108:44–79.
- Berridge KC, Robinson TE. 1998. What is the role of dopamine in reward: hedonic impact, reward learning, or incentive salience? *Brain Res Rev.* 28:309–369.
- Boehler CN, Appelbaum LG, Krebs RM, Hopf JM, Woldorff MG. 2010. Pinning down response inhibition in the brain—conjunction analyses of the Stop-signal task. *Neuroimage.* 52:1621–1632.
- Boehler CN, Hopf JM, Stoppel CM, Krebs RM. 2012. Motivating inhibition-reward prospect speeds up response cancellation. *Cognition.* 125(3):498–503.
- Botvinick M, Braver T. 2015. Motivation and cognitive control: from behavior to neural mechanism. *Annu Rev Psychol.* 66:83–113.
- Braver T. 2012. The variable nature of cognitive control: a dual mechanisms framework. *Trends Cogn Sci.* 16(2):106–113.
- Bundt C, Abrahamse EL, Braem S, Brass M, Notebaert W. 2016. Reward anticipation modulates primary motor cortex excitability during task preparation. *Neuroimage.* 142:483–488.
- Cavanagh JF, Frank MJ. 2014. Frontal theta as a mechanism for cognitive control. *Trends Cogn Sci.* 18(8):414–421.
- Chambers CD, Garavan H, Bellgrove MA. 2009. Insights into the neural basis of response inhibition from cognitive and clinical neuroscience. *Neurosci Biobehav Rev.* 33:631–646.
- Cohen MX. 2014. A neural microcircuit for cognitive conflict detection and signaling. *Trends Neurosci.* 37(9):480–490.
- Cohen MX, Cavanagh JF. 2011. Single-trial regression elucidates the role of prefrontal theta oscillations in response conflict. *Front Psychol.* 2(30):1–12.
- Cousineau D. 2005. Confidence intervals in within-subject designs: a simpler solution to Loftus and Masson's method. *Tutor Quant Methods Psychol.* 1(1):42–45.
- Coxon JP, van Impe A, Wenderoth N, Swinnen SP. 2012. Aging and inhibitory control of action: cortical-subcortical connection strength predicts stopping performance. *J Neurosci.* 32(24):8401–8412.
- Cromwell HC, Schultz W. 2003. Effects of expectations for different reward magnitudes on neuronal activity in primate striatum. *J Neurophysiol.* 89:2823–2838.
- Dayan P, Niv Y, Seymour B, Daw ND. 2006. The misbehavior of value and the discipline of the will. *Neural Netw.* 19:1153–1160.
- De Jong R, Liang CC, Lauber E. 1994. Conditional and unconditional automaticity: a dual-process model of effects of spatial stimulus-response correspondence. *J Exp Psychol Hum Percept Perform.* 20(4):731–750.
- Delorme A, Makeig S. 2004. EEGLAB: an open source toolbox for analysis of single-trial EEG dynamics including independent component analysis. *J Neurosci Methods.* 134(1):9–21.
- Drisdelle BL, Aubin S, Jolicoeur P. 2017. Dealing with ocular artifacts on lateralized ERPs in studies of visual-spatial attention and memory: ICA correction versus epoch rejection. *Psychophysiology.* 54(1):83–99.
- Duque J, Olivier E, Rushworth M. 2013. Top-down inhibitory control exerted by the medial frontal cortex during action selection under conflict. *J Cogn Neurosci.* 25(10):1634–1648.
- Duverno S, Koechlin E. 2017. Rewards and cognitive control in the human prefrontal cortex. *Cereb Cortex.* 27:5024–5039.
- Eimer M. 1995. Stimulus-response compatibility and automatic response activation: evidence from psychophysiological studies. *J Exp Psychol.* 21(4):837–854.
- Figee M, Vink M, de Geus F, Vulink N, Veltman DJ, Westenberg H, Denys D. 2011. Dysfunctional reward circuitry in obsessive-compulsive disorder. *Biol Psychiatry.* 69(9):867–874.
- Forstmann BU, van den Wildenberg WP, Ridderinkhof KR. 2008. Neural mechanisms, temporal dynamics, and individual differences in interference control. *J Cogn Neurosci.* 20:1854–1865.
- Freeman SM, Aron AR. 2016. Withholding a reward-driven action: studies of the rise and fall of motor activation and the effect of cognitive depletion. *J Cogn Neurosci.* 28(2):237–251.
- Freeman SM, Razhas I, Aron AR. 2014. Top-down response suppression mitigates action tendencies triggered by a motivating stimulus. *Curr Biol.* 24:212–216.
- Fries P. 2005. A mechanism for cognitive dynamics: neuronal communication through neuronal coherence. *Trends Cogn Sci.* 9(10):474–480.
- Friston KJ. 2009. Causal modelling and brain connectivity in functional magnetic resonance imaging. *PLoS Biol.* 7(2):e1000033.
- Friston KJ, Fletcher P, Josephs O, Holmes A, Rugg MD, Turner R. 1998. Event-related fMRI: characterizing differential responses. *Neuroimage.* 7:30–40.
- Friston KJ, Harrison L, Penny W. 2003. Dynamic causal modelling. *Neuroimage.* 19:1273–1302.
- Haber SN, Knutson B. 2010. The reward circuit: linking primate anatomy and human imaging. *Neuropsychopharmacology.* 35:4–26.
- Hare TA, Malmaud J, Rangel A. 2011. Focusing attention on the health aspects of foods changes value signals in vmPFC and improves dietary choice. *J Neurosci.* 31(30):11077–11087.
- Herz DM, Christensen MS, Bruggemann N, Hulme OJ, Ridderinkhof KR, Madsen KH, Siebner HR. 2014. Motivational tuning of fronto-subthalamic connectivity facilitates control of action impulses. *J Neurosci.* 34(9):3210–3217.
- Hikosaka O, Isoda M. 2010. Switching from automatic to controlled behavior: cortical-basal ganglia mechanisms. *Trends Cogn Sci.* 14(4):154–161.
- Hommel B. 2011. The Simon effect as tool and heuristic. *Acta Psychol (Amst).* 136(2):189–202.
- Hopfinger J, Büchel C, Holmes AP, Friston KJ. 2000. A study of analysis parameters that influence the sensitivity of event-related fMRI analyses. *Neuroimage.* 11(4):326–333.
- Jahfari S, Waldorp L, van den Wildenberg W, Scholte HS, Ridderinkhof KR, Forstmann BU. 2011. Effective connectivity reveals important roles for both the hyperdirect (fronto-subthalamic) and the indirect (fronto-striatal-pallidal) fronto-basal ganglia pathways during response inhibition. *J Neurosci.* 31(18):6891–6899.
- Jung TP, Makeig S, Westerfield M, Townsend J, Courchesne E, Sejnowski TJ. 2000. Removal of eye activity artifacts from visual event-related potentials in normal and clinical subjects. *Clin Neurophysiol.* 111(10):1745–1758.
- Kang G, Wang L, Zhou X. 2017. Reward interacts with modality shift to reduce cross-modal conflict. *J Vis.* 17(1):19. 114.
- Kouneiher F, Charron S, Koechlin E. 2009. Motivation and cognitive control in the human prefrontal cortex. *Nat Neurosci.* 12:939–945.
- Krebs RM, Boehler CN, Eger T, Woldorff MG. 2011. The neural underpinnings of how reward associations can both guide and misguide attention. *J Neurosci.* 31(26):9752–9759.
- Krebs RM, Boehler CN, Woldorff MG. 2010. The influence of reward associations on conflict processing in the Stroop task. *Cognition.* 117(3):341–347.

- Le Pelley M, Pearson D, Griffiths O, Beesley T. 2015. When goals conflict with values: counterproductive attentional and oculomotor capture by reward-related stimuli. *J Exp Psychol Gen.* 144(1):158–171.
- Leuthold H. 2011. The Simon effect in cognitive electrophysiology: a short review. *Acta Psychol (Amst).* 136:203–211.
- Leuthold H, Jentzsch I. 2002. Distinguishing neural sources of movement preparation and execution: an electrophysiological analysis. *Biol Psychol.* 60:173–198.
- Logan GD. 1994. On the ability to inhibit thought and action: a user's guide to the stop signal paradigm. In: Dagenbach D, Carr TH, editors. *Inhibitory processes in attention, memory, and language.* San Diego: Academic Press. p. 189–239.
- Madsen KS, Baare W, Vestergaard M, Skimminge A, Ejersbo LR, Ramsøy TZ, Gerlach C, Akeson P, Paulson OB, Jernigan TL. 2010. Response inhibition is associated with white matter microstructure in children. *Neuropsychologia.* 48(4):854–862.
- Maris E, Oostenveld R. 2007. Nonparametric statistical testing of EEG- and MEG-data. *J Neurosci Methods.* 164(1):177–190.
- Neubert FX, Mars RB, Buch ER, Olivier E, Rushworth MF. 2010. Cortical and subcortical interactions during action reprogramming and their related white matter pathways. *Proc Natl Acad Sci USA.* 107:13240–13245.
- Nigbur R, Cohen MX, Ridderinkhof KR, Stürmer B. 2012. Theta dynamics reveal domain-specific stimulus and response conflict. *J Cogn Neurosci.* 24(5):1264–1274.
- Oostenveld R, Fries P, Maris E, Schoffelen JM. 2011. FieldTrip: Open source software for advanced analysis of MEG, EEG, and invasive electrophysiological data. *Comput Intell Neurosci.* 2011:156869.
- Padmala S, Pessoa L. 2010. Interactions between cognition and motivation during response inhibition. *Neuropsychologia.* 48(2):558–565.
- Padmala S, Pessoa L. 2011. Reward reduces conflict by enhancing attentional control and biasing visual cortical processing. *J Cogn Neurosci.* 23(11):3419–3432.
- Penny WD, Stephan KE, Mechelli A, Friston KJ. 2004. Comparing dynamic causal models. *Neuroimage.* 22:1157–1172.
- Proctor RW, Miles JD, Baroni G. 2011. Reaction time distribution analysis of spatial correspondence effects. *Psychon Bull Rev.* 18:242–266.
- Rae CL, Hughes LE, Weaver C, Anderson MC, Rowe JB. 2014. Selection and stopping in voluntary action: a meta-analysis and combined fMRI study. *Neuroimage.* 88:381–391.
- Ridderinkhof KR. 2002. Activation and suppression in conflict tasks: empirical clarification through distributional analyses. In: Prinz W, Hommel B, editors. *Common mechanisms in perception and action. Attention and performance.* Oxford: Oxford University Press. p. 494–519.
- Ridderinkhof KR, Forstmann BU, Wylie SA, Burle B, van den Wildenberg W. 2011. Neurocognitive mechanisms of action control: resisting the call of the Sirens. *Wiley Interdiscip Rev Cogn Sci.* 2(2):174–192.
- Ridderinkhof KR, Ullsperger M, Crone EA, Nieuwenhuis S. 2004. The role of the medial frontal cortex in cognitive control. *Science.* 306:443–447.
- Rothkirch M, Schmack K, Deserno L, Darmohray D, Sterzer P. 2014. Attentional modulation of reward processing in the human brain. *Hum Brain Mapp.* 35:3036–3051.
- Rushworth MF, Walton ME, Kennerley SW, Bannerman DM. 2004. Action sets and decisions in the medial frontal cortex. *Trends Cogn Sci.* 8:410–417.
- Salzer Y, de Hollander G, Forstmann BU. 2017. Sensory neural pathways revisited to unravel the temporal dynamics of the Simon effect: a model-based cognitive neuroscience approach. *Neurosci Biobehav Rev.* 77:48–57.
- Shenhav A, Botvinick MW, Cohen JD. 2013. The expected value of control: an integrative theory of anterior cingulate cortex function. *Neuron.* 79(2):217–240.
- Simon JR. 1969. Reactions toward the source of stimulation. *J Exp Psychol.* 81(1):174–176.
- Sommer W, Leuthold H, Hermanutz M. 1993. Covert effects of alcohol revealed by event-related potentials. *Percept Psychophys.* 54:127–135.
- Stephan KE, Penny WD, Daunizeau J, Moran RJ, Friston KJ. 2009. Bayesian model selection for group studies. *Neuroimage.* 46:1004–1017.
- Swann NC, Cai W, Conner CR, Pieters TA, Claffey MP, George JS, Aron AR, Tandon N. 2012. Roles for pre-supplementary motor area and the right inferior frontal gyrus in stopping action: electrophysiological responses and functional and structural connectivity. *Neuroimage.* 59(3):2860–2870.
- Theeuwes J, Belopolsky AV. 2012. Reward grabs the eye: oculomotor capture by rewarding stimuli. *Vis Res.* 74:80–85.
- Töllner T, Rangelov D, Müller HJ. 2012. How the speed of motor-response decisions, but not focal-attentional selection, differs as a function of task set and target prevalence. *Proc Natl Acad Sci USA.* 109(28):1990–1999.
- Töllner T, Wang Y, Makeig S, Müller HJ, Jung TP, Gramann K. 2017. Two independent frontal midline theta oscillations during conflict detection and adaptation in a Simon-type manual reaching task. *J Neurosci.* 37(9):2504–2515.
- Valle-Inclan F, Redondo M. 1998. On the automaticity of ipsilateral response activation in the Simon effect. *Psychophysiology.* 35(4):366–371.
- van Schie HT, Mars RB, Coles MG, Bekkering H. 2004. Modulating of activity in medial frontal and motor cortices during error observation. *Nat Neurosci.* 7(5):549–554.
- van Turennout M, Hagoort P, Brown CM. 1998. Brain activity during speaking: from syntax to phonology in 40 milliseconds. *Science.* 280(5363):572–574.
- Volkow ND, Wang G, Newcorn JH, Kollins SH, Wigal TL, Telang F, Fowler JS, Swanson JM. 2011. Motivation deficit in ADHD is associated with dysfunction of the dopamine reward pathway. *Mol Psychiatry.* 16(11):1147–1154.
- Wang L, Yu H, Hu J, Theeuwes J, Gong X, Xiang Y, Jiang C, Zhou X. 2015. Reward breaks through center-surround inhibition via anterior insula. *Hum Brain Mapp.* 36:5233–5251.
- Wang L, Yu H, Zhou X. 2013. Interaction between value and perceptual salience in value-driven attentional capture. *J Vis.* 13(3):5. 113.
- Wascher E, Schatz U, Kuder T, Verleger R. 2001. Validity and boundary conditions of automatic response activation in the Simon task. *J Exp Psychol Hum Percept and Perform.* 27: 731–751.
- Westbrook A, Braver TS. 2016. Dopamine does double duty in motivating cognitive effort. *Neuron.* 89:695–710.
- Wiegand K, Wascher E. 2005. Dynamic aspects of stimulus-response correspondence: evidence for two mechanisms involved in the Simon effect. *J Exp Psychol Hum Percept Perform.* 31(3):453–464.
- Yee DM, Braver TS. 2018. Interactions of motivation and cognitive control. *Curr Opin Behav Sci.* 19:83–90.
- Zhang J, Kornblum S. 1997. Distributional analysis and De Jong, Liang, and Lauber's (1994) dual-process model of the Simon effect. *J Exp Psychol Hum Percept Perform.* 23(5): 1543–1551.